Solubilization of Various Fluorocarbons in a Fluorinated Surfactant/Water System: Relation with the Design of Porous Materials

R. Bleta, J. L. Blin, and M. J. Stébé*

Equipe Physico-chimie des Colloïdes, UMR SRSMC N° 7565 Université Nancy-1, CNRS, Faculté des Sciences, BP 239, F-54506 Vandoeuvre-les-Nancy Cedex

Received: July 13, 2006; In Final Form: September 12, 2006

We have investigated the phase behavior of the $R^F_7(EO)_8$ surfactant in water as well as the effect of the solubilization of various fluorocarbons in this system. Results show that the cloud point (CP) curve is shifted to high temperatures upon addition of fluorocarbons, following the sequence 1-bromo-perfluorooctane (PFOB) < perfluorodecalin (PFD) < perfluorooctane (PFO). The values of the phase inversion temperature (PIT) associated with these systems increase in the same order: PFOB ∼ 65 °C, PFD ∼ 82 °C, and PFO > 90 °C. Starting from these systems, we have prepared mesoporous and hierarchical porous materials. The formation of the ordered mesoporous materials has been related to the CP curve. Indeed, our results show that mesoporous materials with a high degree of ordering are obtained from systems whose CP curve is shifted toward high temperatures. We have also correlated the formation of the hierarchical porous silica to the PIT. It appears that the design of macro-mesoporous materials is favored with systems that exhibit a high value of the PIT.

1. Introduction

One of the main characteristics of nonionic surfactant compared with the ionic ones is that nonionic surfactant-based systems exhibit a miscibility curve, above which the system separates in two phases. The value of the cloud point (CP) depends strongly on the hydrophilic−lipophilic balance (HLB) number of the surfactant but also on the addition of oil, which involves a shift of the miscibility curve. For example, it has been shown that the addition of C_6H_6 in a 1 wt % solution of $C_9H_{19}C_6H_4$ $(CH_2CH_2O)_{9.2}OH$ decreases the CP from 56 °C to below 0 °C, whereas the addition of *n*-$C_{16}H_{34}$ increases it to 80 °C.[1] Among the nonionic surfactants, the fluorinated ones are of particular interest. Indeed, linear fluorocarbon chains are less flexible than the hydrocarbon ones and, thus, present high melting points. As a consequence, fluorinated surfactants exhibit a higher thermal stability than their hydrogenated analogue. Moreover, by analogy with hydrogenated surfactants, which favor the solubilization of hydrocarbons, the fluorinated ones allow the solubilization of fluorocarbons. This solubilization of oil in water leads to the formation of various structures such as swollen micelles, microemulsions, or emulsions. One important parameter that should be taken into account for the characterization of the surfactant/oil/water ternary system is the phase inversion temperature (PIT). Indeed, at this temperature, the transition from direct systems to reverse ones, where the continuous media is nonpolar, occurs. When the value of the PIT is high, the curvature radius of the surfactant is not reversed, and the Bankroft rule is verified. Thus, the aqueous phase will be the external one and oil-in-water (o/w) concentrated emulsions, which can contain a high quantity of the dispersed phase (oil), can be formulated.

The nonionic surfactants are used in various domains as emulsifiers, wetting agents, detergents, or solubilizers and, more recently, surfactant-based systems have been widely used for the preparation of porous materials. Indeed, for the past few years,[2−8] surfactant templated mesoporous materials as well as their mechanism of formation have been extensively investigated. These materials display a wide range of pore sizes and symmetries that can readily be tailored by adjusting among other factors the physicochemical properties of surfactant or by adding a swelling agent. A lot of interest has been focused on these materials due to their potential applications in catalysis,[9,10] drug delivery,[11] and biosensing,[12−14] for instance. When the mesoporous material is prepared from a micellar solution, it is today well-accepted that the formation of these materials occurs through the cooperative templating mechanism (CTM), which is based on the interactions between the surfactant headgroups and the silicate species in solution.[4,15−17] The structure of the resulting materials is, therefore, strongly related to the behavior of the surfactant in solution, which can be modified by the incorporation of oil. In addition to mesoporous materials, hierarchically porous materials have been synthesized. One way to design such materials consists of using emulsion. In that case, the main role of oil is to act as a template for the generation of the macropore network.[18−21] The characterization of the wall structure of some of these materials has revealed the presence of mesopores, which are found to adopt in most cases a wormhole-like structure and very rarely a hexagonal one.[22,23] The synthesis of macro-cellular silica foams during the natural creaming process of an oil-in-water emulsion has also been reported by Sen et al.[19,20] Anyway, even if recent works have demonstrated the ability of fluorinated surfactants to be employed for the synthesis of highly ordered mesoporous silica,[24−28] most of the investigated surfactant-based systems deal with hydrogenated surfactants. However, the presence of fluorine atoms brings peculiar properties and, in particular, fluorinated surfactants allow the formation of reverse or direct concentrated fluorinated emulsions with high stability, which can contain up to 98% of the dispersed phase (water or fluorocarbon). But, in contrary to the hydrogenated emulsions, the fluorinated ones have not yet been used for the preparation of hierarchical materials. In this study, we have used a series of fluorocarbons to prepare porous silica. As mentioned above, the introduction of organic auxiliaries strongly affect the surfactant behavior in

10.1021/jp0644199 CCC: $33.50
Published on Web 10/25/2006

solution and, thus, the characteristics of the porous structures. For that purpose, in a first part, we have undertaken a detailed study of the phase behavior of the surfactant/oil/water systems, and in particular, we have investigated the ability of various fluorocarbons to form o/w emulsions.

2. Experimental Section

The surfactant used in the present study was provided by Dupont and used without further purification. It has an average chemical formula of $C_7F_{15}C_2H_4(OC_2H_4)_8OH$, labeled as $R^F_7(EO)_8$. The hydrophilic and hydrophobic moieties of this surfactant exhibit a Gaussian chain length distribution. Perfluorooctane (PFO), perfluorodecalin (PFD), and 1-bromo-perfluorooctane (PFOB) were provided by Aldrich.

Phase Diagram Determination: The phase diagrams have been established by preparing samples over the whole range of surfactant/water compositions. The required amounts of surfactant, oil, and water were introduced into well-closed glass vials to avoid evaporation. The samples were placed in a thermostatic bath and, depending on the system, they were allowed to stand from a few hours to several days at the temperature of interest to reach equilibrium. The different phases were identified by visual inspection with a polarizing light microscope (Olympus BX 50). Micelles were characterized by rheological experiments, and the average hydrodynamic radius of the microemulsion droplets was measured by dynamic light scattering with a Malvern 300HSA Zetasizer instrument. The boundary lines of the liquid crystal domains were evidenced by small-angle X-ray scattering (SAXS) experiments.

Pseudo-Shinoda diagrams have been established to determine the solubility of the three fluorocarbons in the aqueous solution of surfactant as a function of the temperature, according to the method previously used by Shinoda.[29] These diagrams are drawn for various water/surfactant weight ratios (R) for the investigated fluorocabons.

Preparation of Porous Materials: First, a micellar solution was prepared with 25 wt % of $R^F_7(EO)_8$ dissolved in a 0.01 M aqueous solution of sulfuric acid. The oil compositions were chosen to be either in the microemulsion domain or in the emulsion region, and the concentration of oil was varied from 0 to 60 wt %. The mixtures were homogenized by stirring before the addition of tetramethoxysilane (TMOS). TMOS was added dropwise at 40 °C, and the solutions were kept under stirring for 1 h. The water/surfactant weight ratio and the $R^F_7(EO)_8$/silica molar ratio were respectively fixed at 3 and 0.5. The obtained mixtures were sealed in Teflon autoclaves and allowed to undergo hydrothermal treatment at 80 °C for 24 h. Ethanol extraction was carried out with a Soxhlet apparatus for 48 h.

Characterization of Porous Materials: The structure of the recovered materials was characterized by SAXS experiments, using a home built apparatus equipped with a classical tube ($\lambda = 1.54$ Å). The X-ray beam was focused by means of a curved gold/silica mirror on the detector, which was placed at 527 mm from the sample holder. The scattering profiles were acquired with a one-dimensional position-sensitive detector. Nitrogen adsorption−desorption isotherms were obtained at −196 °C, over a wide relative pressure range from 0.01 to 0.995, with a volumetric adsorption analyzer TRISTAR 3000 manufactured by Micromeritics. The samples were degassed under vacuum for several hours at 320 °C before nitrogen adsorption measurements. The pore diameter and the pore size distribution were determined by the BJH (Barret, Joyner, and Halenda) method.[30] Although it is well-known that this method gives an underestimated pore size and that some new methods have been developed,[31] we used it here for the sake of simplicity, and this mathematical algorithm does not significantly affect the results as it is a systematic comparison. Scanning electron microscopy was carried out with a Hitachi S-2500 at 15 keV.

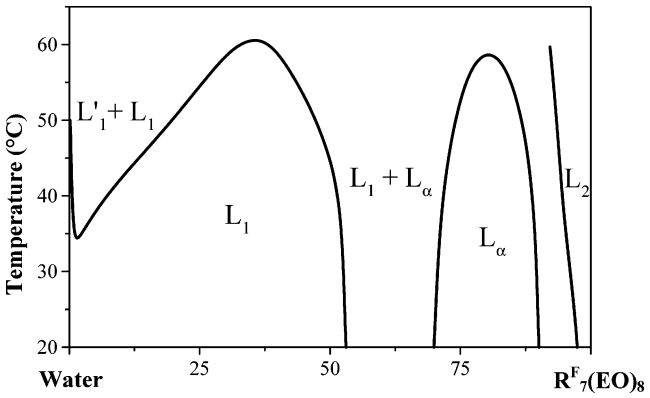

Figure 1. Temperature−composition phase diagram of $R^F_7(EO)_8$ in water.

3. Results and Discussion

3.1. Binary Phase Diagram. The binary surfactant/water phase diagram (Figure 1), which has been established between 20 and 65 °C, evidenced that $R^F_7(EO)_8$ presents a CP at 34 °C for 1 wt % of surfactant. Below the miscibility curve, the system is thermodynamically stable and presents a uniform single isotropic phase (L_1), whereas above this curve, the phase separation occurs and the system separates into two phases: one phase rich in micelles (L_1) and the other one poor in micelles of surfactant (L'_1). The isotropic micellar phase L_1 is found to be present over a wide range of surfactant compositions going up to 52.5 wt % at 20 °C. The liquid crystal domain contains only a lamellar (L_α) phase, which is stable over a temperature range going up to 57.5 °C.

The micellar solutions prepared at 25 wt % of surfactant showed flow birefringence, while remaining isotropic at rest. When the micelles were characterized by birefringence experiments under weak shear flows at 22 °C they exhibited an elongated shape with a length in the range of 320−340 nm for a width fixed at 7 nm.

3.2 Incorporation of Fluorocarbons in the $R^F_7(EO)_8$/Water System. *3.2.1. Ternary Phase Diagrams.* Figure 2 shows phase diagrams of the $R^F_7(EO)_8$/fluorocarbon/water systems at 20 °C. At this temperature, micelles can incorporate up to 6 wt % of PFO (Figure 2A) and up to 12 wt % of PFD (Figure 2B). Concerning PFOB, the situation is quite different; 4 wt % of oil can be incorporated in the micelles, and for higher concentrations of PFOB, a domain of microemulsion, which joined the water corner, is also detected (Figure 2C). These microemulsions can incorporate up to 21 wt % of PFOB at 20 °C. Whatever the type of oil, hexagonal (H_1) and micellar cubic (I_1) phases appear only upon addition of oil, whereas the L_α phase, which exists in the binary system, swells. Even if these three diagrams are similar in terms of phase sequences, we should note that the amount of PFO (Figure 2A) incorporated in the liquid crystal phases is lower than that of PFD (Figure 2B) and that of PFOB (Figure 2C).

On the other hand, at high oil amounts (oil-rich corner of the phase diagram), very stable concentrated emulsions are formed with the PFO- and PFD-based systems at 20 °C, whereas PFOB does not form concentrated emulsions at this temperature. For example, the samples prepared at $R = 5.7$, with 95 wt % of PFOB, were fluid and split into two phases, whereas those

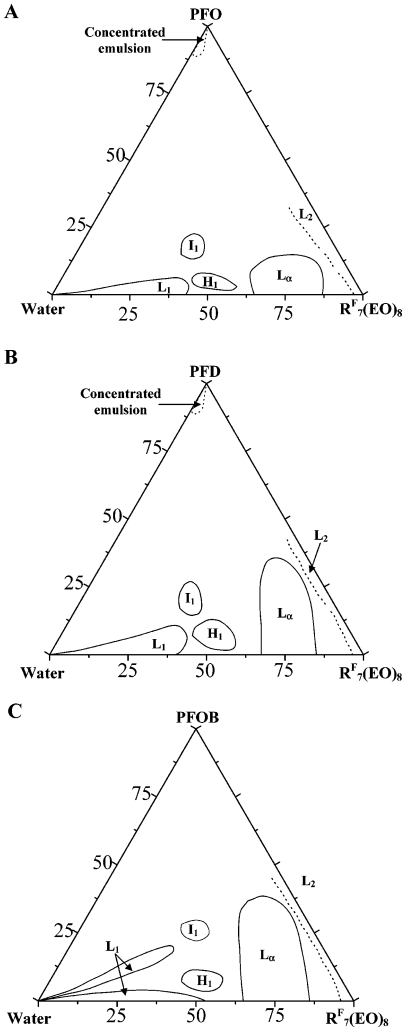

Figure 2. Phase diagram (wt %) of $R^F_7(EO)_8$/fluorocarbon/water system at 20 °C. A, PFO; B, PFD; and C, PFOB.

prepared with PFD and PFO appeared highly viscoelastic and very stable for months. PFOB is, therefore, not an efficient fluorocarbon to form stable concentrated emulsions with the surfactant $R_7^F(EO)_8$.

3.2.2. Properties of Solubilization of the Investigated Fluorocarbons. The solubilization of the investigated fluorocarbons in the $R_7^F(EO)_8$/water system was studied according to a method previously used by Shinoda and Ogawa.[29] This method consists of determining the miscibility curves versus the temperature (Figure 3). The isotropic phase obtained for each water/surfactant ratio is limited by two curves. The lower curve, shown by the open circles, is the solubilization curve above which microemulsions form. The upper curve, shown by the solid circles, is the CP curve. When the mixtures were brought at temperatures above this latter curve, they appeared macroscopically biphasic, comprising a lower viscous and whitish phase and an upper fluid and transparent phase. Because fluorocarbons have a higher specific gravity than that of water (approximately twice that of water), the oil-rich phase settles in the bottom of the mixture. A careful observation of the lower phase by optical microscopy indicated the presence of an oil-in-water emulsion whose structure was similar to that of concentrated emulsions formed with very high volume fractions of PFD (>90%).[33] While the equilibrium time to establish the solubilization curve was rather long (in particular at high oil amounts), the CP curve was easily obtained, and the samples turned opaque instantaneously. This latter phenomenon was reversible, and after cooling the mixtures, a single isotropic phase was obtained again, whereas it took a long time before reaching the demixion

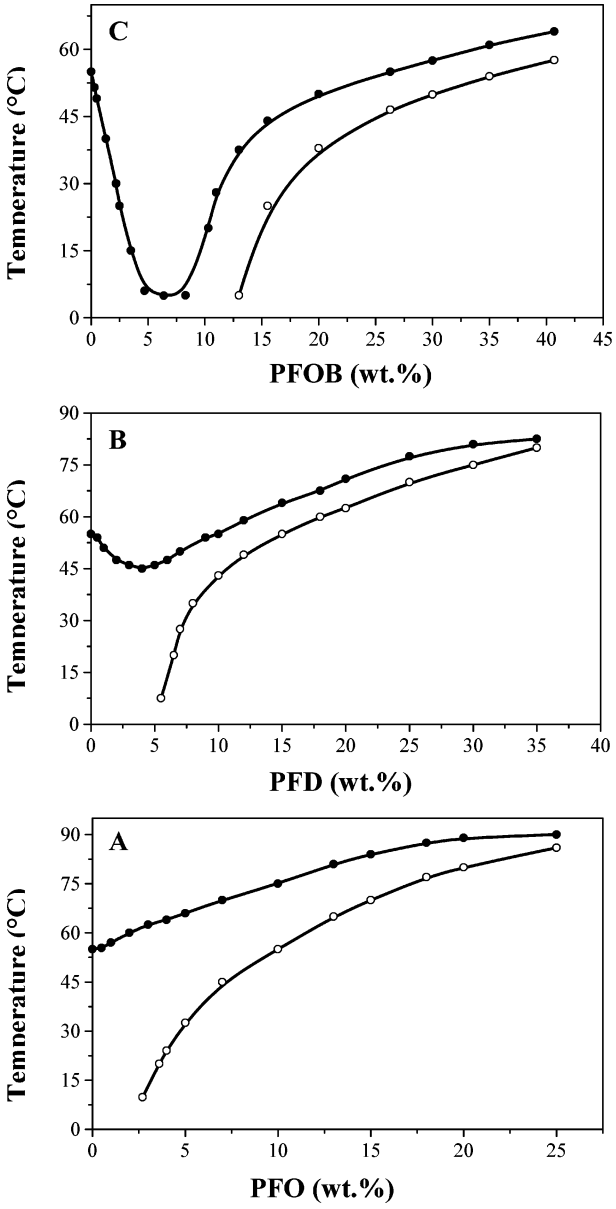

Figure 3. Pseudo-Shinoda diagrams established for a water/surfactant ratio equal to 3 and with A, PFO; B, PFD; and C, PFOB.

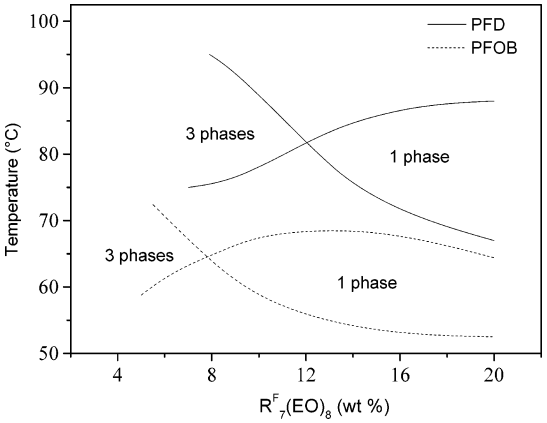

Figure 4. PIT determination: Minimum surfactant requirement to obtain an isotropic solution containing fluorocarbon and water in a 1:1 weight.

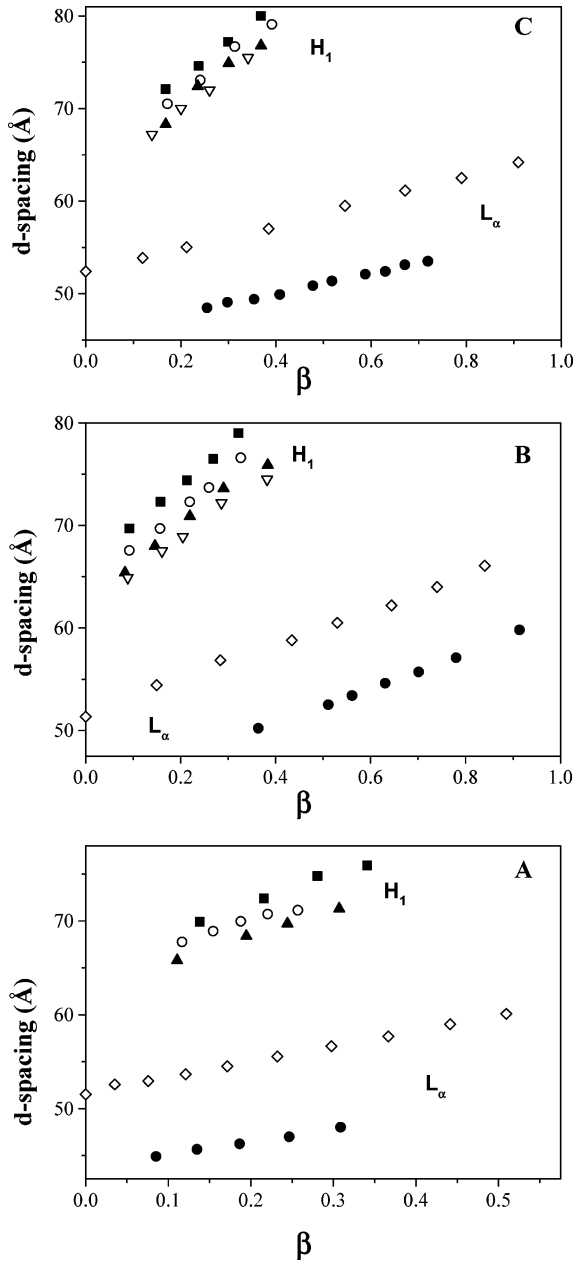

Figure 5. $R^F_7(EO)_8$/fluorocarbon/water system: Evolution of the *d* spacing as a function of β, the number of oil molecules per surfactant molecule, in the hexagonal (H_1) and lamellar (L_α) phases for different values of water/$R^F_7EO_8$ weight ratio (*R*). ■, $R = 1$; ○, $R = 0.91$; ▲, $R = 0.82$; ▽, $R = 0.75$; ◇, $R = 0.25$; and ●, $R = 0.11$. A, PFO; B, PFD; and C, PFOB.

of the microemulsions by cooling. We consequently established, for various oils, the pseudo-Shinoda diagrams by heating the samples. By comparing the three diagrams, represented in Figure 3, a shift of the CP curve to higher temperatures is observed following the sequence: PFOB < PFD < PFO. This suggests that compared to PFD and PFO, PFOB interacts more strongly with the oxyethylene groups, and as a consequence, the system becomes more hydrophobic.[34] Such a behavior could be explained by the presence of the highly polarizable terminal bromide atom, which brings a higher degree of lipophilicity.[35]

The solubility of fluorocarbons in aqueous solutions of surfactant has been described in terms of PIT. PIT can be determined from the temperature at which the minimum concentration of surfactant is used to solubilize equal weights

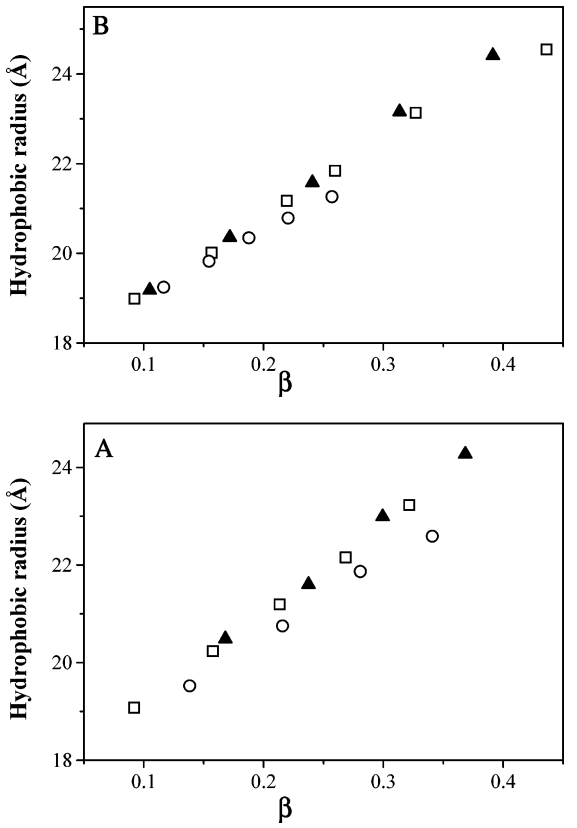

Figure 6. Hexagonal liquid crystal $R^F_7(EO)_8$/fluorocarbon/water system: Evolution of the hydrophobic radius (R_H) as a function of β for $R = 1$ (A) and $R = 0.9$ (B). ○, PFO; □, PFD; and ▲, PFOB.

of water and oil in a single isotropic phase.[36] The PITs of the investigated systems were determined from the diagrams represented in Figure 4 and were found to increase in the order PFOB ∼ 65 °C, PFD ∼ 82 °C, and PFO > 90 °C. These values are in good agreement with the empirical formula established to predict the PIT value in fluorinated systems[37]

$$\text{PIT (°C)} = 31\text{HLB} + 1.7\text{ECN} - 225$$

where the ECN (equivalent carbon number) characterizes the fluorocarbon and depends on its structure, whereas the HLB is specific to the surfactant. Indeed, with a HLB value of 9.6 for $R_7^F(EO)_8$, the calculated PITs are found to be equal to 67 °C for PFOB, 83 °C for PFD, and 86 °C for PFO.

The size of the oil-swollen micelles was also measured by dynamic light scattering experiments. The samples were prepared from microemulsion with a *R* value equal to 3 and containing, respectively, 3 and 4 wt % of PFD and PFOB. Then, these solutions were diluted to reach a dispersed volume fraction between 5×10^{-3} and 0.03 w/w. The results indicate that micelles have a diameter of about 11 and 13 nm, respectively, suggesting a progressive evolution of the micelle shape from wormlike to a spheroid drop upon addition of oil. Indeed, it should be reminded that birefringence experiments have shown that, in water, $R_7^F(EO)_8$ micelles exhibited an elongated shape.

3.2.3. Liquid Crystal Phases: Figure 5 shows the evolution at 20 °C of the *d* spacing characteristic of the degree of swelling of the liquid crystalline phase as a function of β, the number of oil molecules per surfactant molecule, for different values of *R*. For the sake of clarity, the three types of oil are represented separately.

Hexagonal Phase: The addition of small quantities of fluorocarbon to the binary $R^F_7(EO)_8$/water system induced the

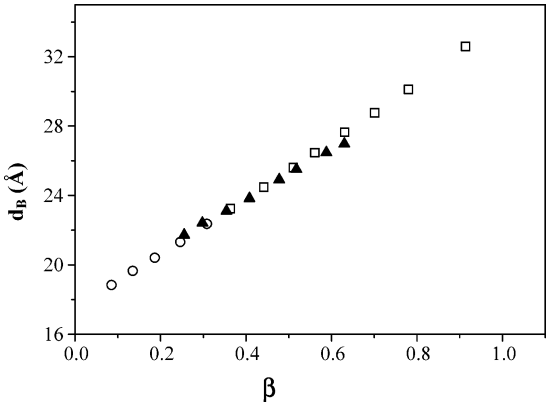

Figure 7. Lamellar liquid crystal $R^F_7(EO)_8$/fluorocarbon/water system: Evolution of the hydrophobic (d_B) thickness of the surfactant chain as a function of β for $R = 0.11$. ○, PFO; □, PFD; and ▲, PFOB.

formation of the hexagonal phase, which consists of infinitely long cylinders packed in a hexagonal array. The hexagonal structure is characterized by three Bragg reflections whose positions are in the ratio $1:\sqrt{3}:2$. Because the hexagonal phase does not exist in the binary system, the value of d spacing at $\beta = 0$ is not shown in the graphic. As the fraction of added oil is increased, the hexagonal structure swells continuously (d increases) until the maximum equilibrium swelling is reached. Beyond this maximum, the structure expels the excess of oil and the d spacing does not increase anymore. For example, for $R = 1$ (solid squares), this occurs for approximately $\beta = 0.28$, $\beta = 0.32$, and $\beta = 0.36$, giving rise to a maximum d spacing of 74.8, 79.2, and 80.1 Å in PFO (Figure 5A), PFD (Figure 5B) and PFOB (Figure 5C) systems, respectively. The value d_{100} is given by the first reflection and, in the H_1 phase, it is related to the radius of the hydrophobic core (R_H) by the following relation[38]

$$\frac{V_B + \beta V_O}{V_S + \alpha V_W + \beta V_O} = \frac{\sqrt{3}\pi R_H^2}{2d^2}$$

where α and β are the numbers of water and oil molecules, respectively, per surfactant molecule and V_B, V_S, V_W, and V_O are the molar volumes of the hydrophobic part of the surfactant ($V_B = 248$ cm^3/mol), the surfactant ($V_S = 551$ cm^3/mol), water ($V_W = 18$ cm^3/mol), and oil [$V_O = 247$ cm^3/mol (PFO), 237 cm^3/mol (PFD), 256 cm^3/mol (PFOB)]. From Figure 6, which depicts the evolution of the hydrophobic radius as a function of β for various values of R, we can observe, in all cases, an increase of R_H with the incorporation of oil.

The cross sectional area (S) per surfactant molecule can then be deduced from the following relation[38]

$$S = \frac{2(V_B + \beta V_O)}{N_A R_H}$$

where N_A is the number of Avogadro. S remains constant upon addition of PFD ($S = 47.5 \pm 1.0$ Å^2) and PFOB ($S = 47.5 \pm 1.0$ Å^2), while it increases slightly from 47.5 to 49.0 ± 1.0 Å^2 when PFO is incorporated. Assuming that for a given value of R, the conformation of the hydrophobic chains remains unchanged with the incorporation of oil, the values of the cross-sectional area suggest that PFD and PFOB molecules are solubilized essentially in the core of the cylinders, whereas PFO molecules tend to penetrate also in the palisade layer.

Lamellar Phase: The lamellar phase consists of infinitely wide bimolecular layers stacked in a parallel way. The diffraction pattern of such a phase exhibits two reflections associated to the planes of indices 100 and 200. The repetition distance corresponds to the layer spacing between the water and the oil films separated by the surfactant bilayer. Based on geometrical considerations, the cross-sectional area can be calculated from the following formula[38]

$$S = \frac{2(V_S + \alpha V_W + \beta V_O)}{N_A d}$$

In the absence of oil, the surface per polar head of surfactant was found to be equal to 47.5 ± 1 Å^2 and to be independent of the surfactant concentration. It remains constant upon addition of PFD, and no strong deviation from the binary system is observed. Thus, PFD molecules form a free film in the core of

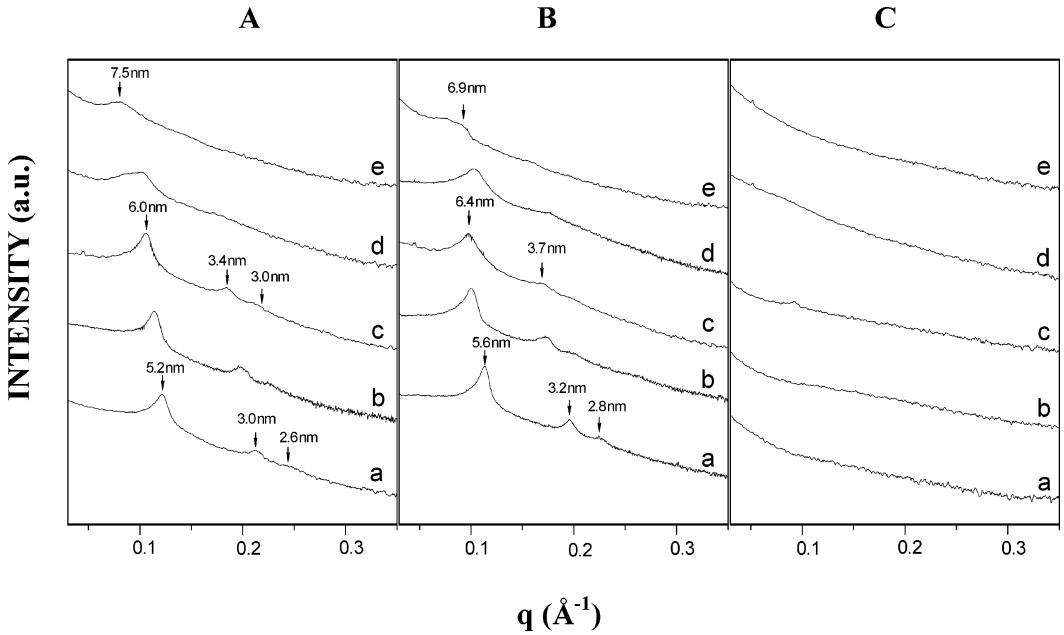

Figure 8. Porous materials: SAXS patterns of samples synthesized with a, 1.5; b, 5; c, 7; d, 20; e, 30 wt % of PFO (A); a, 5; b, 9; c, 12; d, 15; e, 30 wt % of PFD (B); and a, 1; b, 3; c, 10; d, 20; e, 30 of PFOB (C).

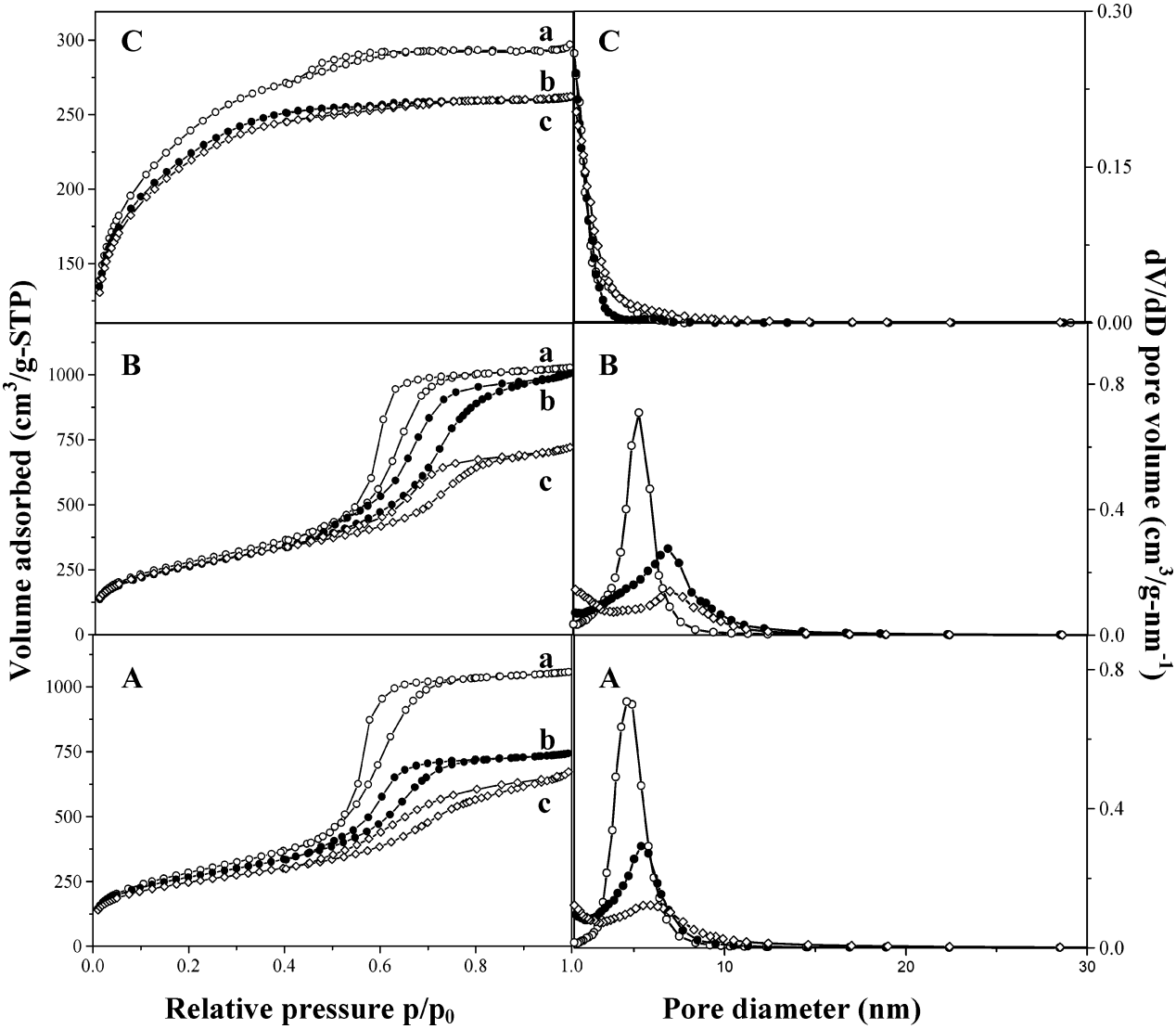

Figure 9. Porous materials: Adsorption−desorption isotherms and pore size distribution of compounds synthesized with a, 1.5; b, 10; c, 30 wt % of PFO (A); a, 3; b, 20; c, 30 wt % of PFD (B); and a, 3; b, 17; c, 30 wt % of PFOB (C).

the bilayer. On the other hand, S increases slightly with β in the PFO system (from 47.5 to 48.5 Å^2) and more significantly in the PFOB system (from 47.5 to 50.7 Å^2), suggesting that PFO and PFOB form an interstitial film of oil in the bilayer of the surfactant fluorinated chains, but these molecules are also penetrated between the fluorinated chains. The hydrophobic thickness (d_B) is calculated from the following relation[38]

$$d_B = \frac{2(V_B + \beta V_O)}{S}$$

Whatever the type of oil, d_B increases regularly with β (Figure 7). The hydrophobic thickness of surfactant chains determined by the extrapolation at $\beta = 0$ gives $d_B = 17.5 \pm 0.5$ Å from which we compute a hydrophobic chain length of $L_B = d_B/2 = 8.7 \pm 0.5$ Å. This value corresponds to that found in the L_α phase of the binary system. By comparing this value to that of a chain with 9 carbon atoms (12.6 Å) we can deduce that hydrophobic chains are semi-extended in the L_α phase.

3.3. Porous Materials. The SAXS pattern of the material prepared in the absence of oil (not shown) exhibits a single broad reflection, indicating the arrangement of the channels into a wormhole-like structure. A type IV isotherm is obtained by nitrogen adsorption−desorption analysis. The specific surface area value is 1030 m^2/g. The pore diameter distribution determined by using the BJH method is quite narrow and centered at about 3.8 nm. Figures 8 and 9 report, respectively, the SAXS patterns and the nitrogen adsorption−desorption isotherms of materials prepared with addition of fluorocarbons.

3.3.1. Materials Prepared with a Low Concentration of Fluorocarbons. Upon addition of PFO, three reflections at d spacing ratios 1:$\sqrt{3}$:2, consistent with a hexagonal symmetry, are observed on the SAXS pattern (Figure 8A, a−c). According to the Bragg's law, the unit cell dimension ($a_0 = 2d_{100}/\sqrt{3}$), which corresponds to the sum of the pore diameter and the thickness of the pore wall, can be calculated, and its values varies from 6.0 to 7.0 nm with the increase in PFO loading from 1.5 to 15 wt %. Similar results are obtained with the incorporation of PFD (Figure 8B, a−d). The situation is quite different in the PFOB system (Figure 8C, a−d), where no line is observed, indicating a further loss of ordering as compared to the samples prepared from the $R_7^F(EO)_8$/water binary system.

A type IV isotherm with a H_1 hystheresis loop by BDDT classification[39] is obtained for the samples prepared from the $R_7^F(EO)_8$/PFO/water or $R_7^F(EO)_8$/PFD/water systems, with a low concentration of oil (Figure 9A, a and b and 9B, a and b). A strong uptake of N_2 adsorption is observed at approximately

TABLE 1: Structural Properties of the Samples Prepared with the Three Fluorocarbons[a]

oil	wt %	structure	*d* (nm)	a_0 (nm)	S_{BET} (m^2/g)	pore diameter (nm)	wall thickness (nm)
PFO	0	wormhole			1030	3.8	
	1.5	hexagonal	5.2	6.0	1002	4.3	1.7
	3	hexagonal	5.3	6.1	1038	4	2.1
	5	hexagonal	5.5	6.3	1009	5	1.3
	7	hexagonal	6.0	6.9	1033	5.2	1.7
	15	hexagonal	6.1	7.0	1002	5.4	1.6
	20	wormhole	-		913	5.4	
	30	wormhole			874	5.6	
	35	wormhole			949	5.2	
	40	wormhole			823	5.2	
	50	wormhole			775		
PFD	0	wormhole			1030	3.8	
	3	hexagonal	5.3	6.1	1018	4.6	1.5
	5	hexagonal	5.6	6.5	1038	4.7	1.8
	7	hexagonal	5.8	6.7	1029	4.9	1.8
	9	hexagonal	6.3	7.3	1000	5.1	2.2
	12	hexagonal	6.4	7.4	1016	5.6	1.8
	15	wormhole	6.4	7.4	1020	5.6	1.8
	30	wormhole			965	7.1	
	35	wormhole			942	7.5	
	50	wormhole			924	8.4	
	60	wormhole			959	8.3	
PFOB	0	wormhole			1030	3.8	
	1	wormhole			840		
	3	wormhole			834		
	10	wormhole			775		
	15	wormhole			760		
	20	wormhole			793		
	30	wormhole			810		
	40	wormhole			806		

[a] Structure, *d* spacing (*d*), unit cell (a_0), specific surface area (S_{BET}), pore diameter, and wall thickness.

$p/p_0 = 0.5-0.65$, which is a result of the filling of the mesopores due to the capillary condensation. The plateau is reached at approximately $p/p_0 = 0.7-0.8$. Beyond this value, the adsorbed volume at the saturation remains constant. As compared to PFO and PFD, the molecular sieves obtained from the $R_7^F(EO)_8$/PFOB/water system exhibit a different behavior (Figure 9C, a and b). Indeed, isotherms are intermediates between type I and IV. According to Dubinin,[40] these kinds of isotherms are characteristic of supermicroporous materials, that is, the pore size is located at the limit between the micro and the mesoporous domain. This phenomenon is further confirmed by the analysis of the pore size distribution, whose maximum is lower than 1.7 nm.

From Table 1, we can observe that the maximum of the pore size distribution is continuously shifted from 3.8 to 5.6 nm upon addition of PFD. If PFO is employed as oil, first the pore diameter increases from 3.8 to 5.0 nm when the concentration of PFO is varied from 0 to 5 wt %, indicating that in this range of concentration, PFO acts as an expander. Beyond 5 wt %, the pore size remains constant, meaning that the swelling of the micelles has reached the maximum. Whatever the type of oil and its loading, the specific surface area is rather high (>750 m^2/g). However, its value slowly decreases with the incorporation of oil.

3.3.2. Materials Prepared with an Intermediate or a High Concentration of Fluorocarbon. If the concentrations of PFO and PFD are higher than 20 wt %, no secondary reflections are any longer detected on the SAXS pattern (Figure 8A, d and e; 8B, e), meaning that the regular channel array is lost; the presence of a single reflection indicates the formation of a disordered structure. As the amount of oil is increased, a change in the shape of the isotherms is observed. At high relative pressures (beyond $p/p_0 = 0.9$), the adsorbed volume of nitrogen does not remain constant anymore (Figure 9A, c and 9B, c). SAXS patterns (Figure 8C, e) and nitrogen adsorption−desorption isotherms (Figure 9C, c) of samples prepared from the $R_7^F(EO)_8$/PFOB/water system remain unchanged with the increase of the PFOB concentration.

From Figure 10, which shows several representative scanning electron micrographs (SEM) of the synthesized silicas, it appears that both $R_7^F(EO)_8$/PFO/water and $R_7^F(EO)_8$/PFD/water systems provide a macroporous network. Indeed, highly porous particles are clearly evidenced. It should be noted that PFO tends to form hollow spheres with apertures whose diameters range from 1 to 7 μm (Figure 10A, a−d). Depending on the fluorocarbon amount, PFD gives rise either to macro-mesoporous structures with polyhedral cells without any interconnecting window (Figure 10B, a) or to big particles of about 30−130 μm in length with oval shapes (Figure 10B, b−d). In any case, the macropores are not well-ordered, and typically, the pore size is in the range of a few microns. The presence of macropores in the samples was confirmed by mercury intrusion experiments. Figure 11 shows the macropore size distribution of the samples prepared at high amounts of oil. The mercury porosimetry does not provide the macroscopic void spaces but rather the window that connects two adjacent macropores. At 40% of PFO (Figure 11a), the sample exhibits a broad peak centered at ~0.8 μm, which corresponds approximately to the size of the interconnected pores observed by SEM (Figure 10A). In addition to the first peak located at ~0.54 μm, the sample prepared at 50% of PFD (Figure 11b) exhibits a second peak situated at ~11 μm. We believe that this second peak arises from the interparticle porosity induced by the aggregation of particles, because no pore size comparable to 11 μm was observed by SEM (Figure 10B). On the other hand, the sample prepared at 40% of PFOB (Figure 11c) exhibits no macroporosity in accordance with SEM analysis (Figure 10C).

3.4. Discussion. Two main tendencies can be drawn from the analysis of the results reported above. First, the incorporation of a low fraction of PFD or of PFO involves the formation of well-ordered mesoporous materials. Second, at intermediate or at high concentrations of these oils, the regular channel array of the mesopore network is lost, but hierarchical macro-mesoporous materials are formed. Moreover, the incorporation of PFOB neither leads to well-ordered mesostructures nor to hierarchical materials.

According to the phase diagram of the $R^F_7(EO)_8$/water system and to the evolution of this diagram with the incorporation of PFD and PFO, micelles or microemulsion are detected. So, the formation of disordered mesostructures when syntheses are carried out from the binary system cannot be related to the perturbation of the CTM mechanism because all conditions are together in order that such a mechanism occurs. Looking at these systems (Figures 1, 2A, and 2B), we rather consider the CP curve to explain this behavior. Indeed, for 25 wt % of surfactant, the CP of $R^F_7(EO)_8$/water is found at 55 °C. When PFD and PFO are added to the micellar solution, the CP curve is shifted toward higher temperatures from 55 to 80 °C for PFD and from 55 to 90 °C for PFO for a water/surfactant ration equal to 3 (Figure 3), and ordered molecular sieves are prepared.

If we consider now the PFOB system, the behavior is quite different. Indeed, only disordered supermicroporous materials are obtained. A possible origin of such behavior could be attributed to the CP curve obtained in the PFOB system. From

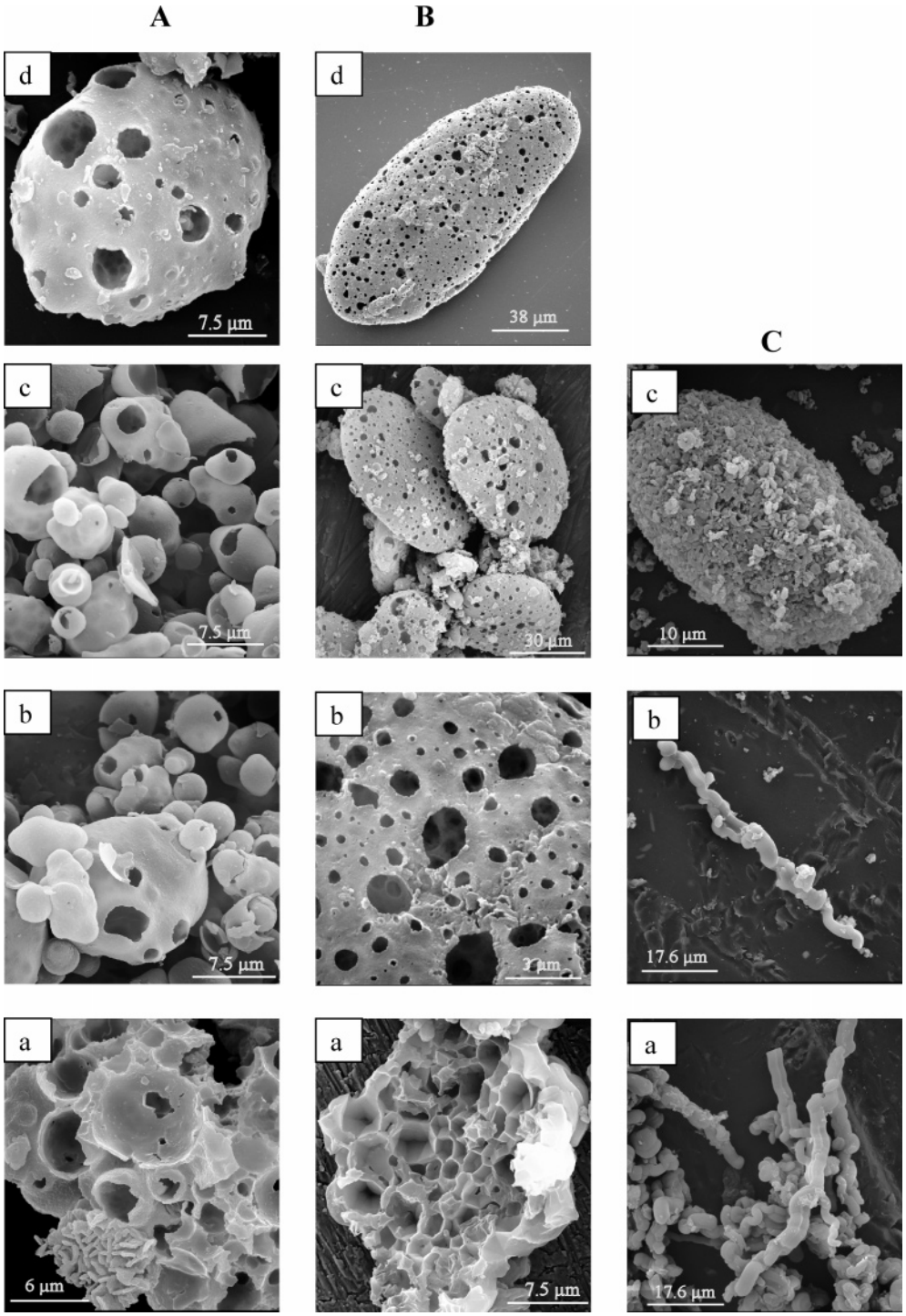

Figure 10. Porous materials: SEM micrograph of samples prepared with a, 20; b, 30; c, 35; d, 40 wt % of PFO (A); a, 15; b, 30; c, 40; d, 50 wt % of PFD (B); and a, 15; b, 15; c, 30 wt % of PFOB (C).

Figure 3C, we can note that with the solubilization of this fluorocarbon the CP curve is first shifted toward lower temperatures up to 5 °C and then it increases up to 55 °C when the maximum incorporation of PFOB is reached. These observations led us to conclude that the CTM mechanism is not favored if the CP is too low. Such a result is in accordance with the one obtained by Kipkemboi et al.,[41] suggesting that a higher degree of mesoporous ordering is obtained when the CP is shifted to higher temperatures.

To explain the second tendency, that is, the fact that the further incorporation of PFD or PFO leads to the formation of the macro-mesoporous silica once again, we should have a look at the diagrams reported in Figure 2A,B. Indeed, the phase behavior of the ternary $R_7^F(EO)_8$/PFD/water and of the R_7^F-$(EO)_8$/PFO/water systems shows that, beyond 6 wt % of PFO and 12 wt % of PFD, the oil is not incorporated into the micelles anymore. Quickly, two phases appear in the vessel. Moreover, for high volume fractions of oil, stable concentrated oil-in-water emulsions are produced. The structure of these emulsions can be described as foams, where the oil droplets covered with a surfactant film bathe in the continuous phase, which is constituted by an o/w microemulsion.[33] The size of the oil

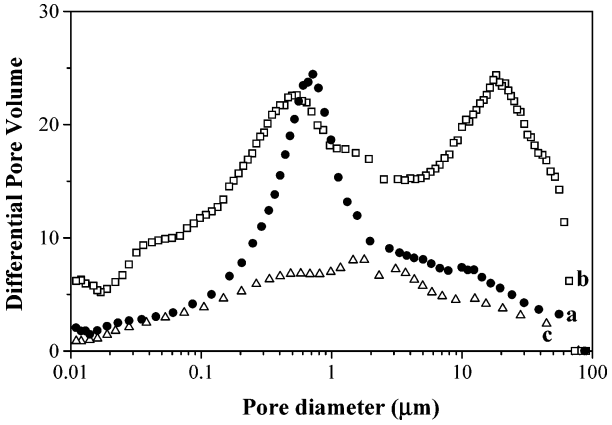

Figure 11. Porous materials: Pore size distributions, determined by mercury intrusion of samples prepared with a, 40 wt % of PFO; b, 50 wt % of PFD; and c, 40 wt % of PFOB.

droplets of the emulsions was determined with an optical microscope. Figure 12 shows the structure of dilute and concentrated emulsions prepared at intermediate (~12 wt %, photo a) and high (~40 wt %, photo b) concentrations of PFD. The dilute emulsion contains droplets of an approximately 2−5 μm diameter that assemble into grapes, whereas the concentrated one is made up of droplets standing close to each other and having approximately the same diameter. The addition of TMOS into these systems leads to the direct preparation of hierarchically structured macroporous-mesoporous silicas. The mechanism of formation of these hierarchical materials can be explained by a combination of the CTM mechanism, which governs the formation of the mesopore network and a templating process, in which the silica source interacts with the surfactant surrounding the deformed oil droplets, creating casts of the morphological macropores. In contrast to PFD and PFO systems, whatever the amount of PFOB, no hierarchical materials are recovered. A possible origin of the peculiar behavior of the PFOB system could be associated with the fact that PFOB does not form stable concentrated emulsions with $R^F_7(EO)_8$ due to its too low PIT. Indeed, to obtain direct concentrated emulsions, the system should exhibit a high value of PIT.[42] In the PFO- and PFD-based systems at intermediate and high concentrations of fluorocarbons, oil droplets of the emulsions coexist with microemulsion, whereas in the PFOB system, the emulsions are not stable, and the coalescence of the oil droplets probably occurs before the polymerization of TMOS takes place. These observations led us to conclude that the design of macro-mesoporous materials is favored with systems that exhibit a high value of PIT.

4. Conclusion

We have investigated the effect of the solubilization of PFO, PFD, and PFOB into the $R_7^F(EO)_8$/water system. Micelles of $R_7^F(EO)_8$ can incorporate at 20 °C up to 6 wt % of PFO and up to 12 wt % of PFD. Concerning the PFOB-based system, the situation is quite different. Indeed, only 4 wt % of oil can be incorporated in the micelles. However, for higher concentrations of PFOB, a domain of microemulsion, which joined the water corner, is also detected. This microemulsion domain can incorporate up to 21 wt % of PFOB at 20 °C. The CP curve is shifted to higher temperatures upon addition of fluorocarbons, following the sequence PFOB < PFD < PFO. PITs were determined and were found to increase in the order PFOB ~ 65 °C, PFD ~ 82 °C, and PFO > 90 °C. We have also delimited the crystal phase domains, and we have determined the structural parameters of these liquid crystal phases.

In regard to the porous materials syntheses, the incorporation of a low fraction of PFD or of PFO leads to the formation of well-ordered mesostructures through a CTM-type mechanism, whereas only disordered supermicroporous materials are recovered when PFOB is used as oil. The difference in such a behavior between these three fluorocarbons can be explained by considering the CP curve. The CTM mechanism is not favored if the CP is not shifted toward higher temperatures. If the concentration of PFO or PFD is further increased, the ordered array of the mesoporous network is lost, but hierarchical porous materials are obtained. The mesopores are generated by the fluorinated micelles, whereas the macropore-network is templated by the oil droplets dispersed in the continuous medium. By contrast, due to its low PIT, no macro-mesoporous material can be prepared from the $R_7^F(EO)_8$/PFOB/water system.

Acknowledgment. Authors would like to thank DuPont de Nemours Belgium for providing the fluorinated surfactant, as well as J. P. Decruppe of the Laboratoire de Physique des Milieux Denses of Université Paul Verlaine Metz for the birefringence experiments.

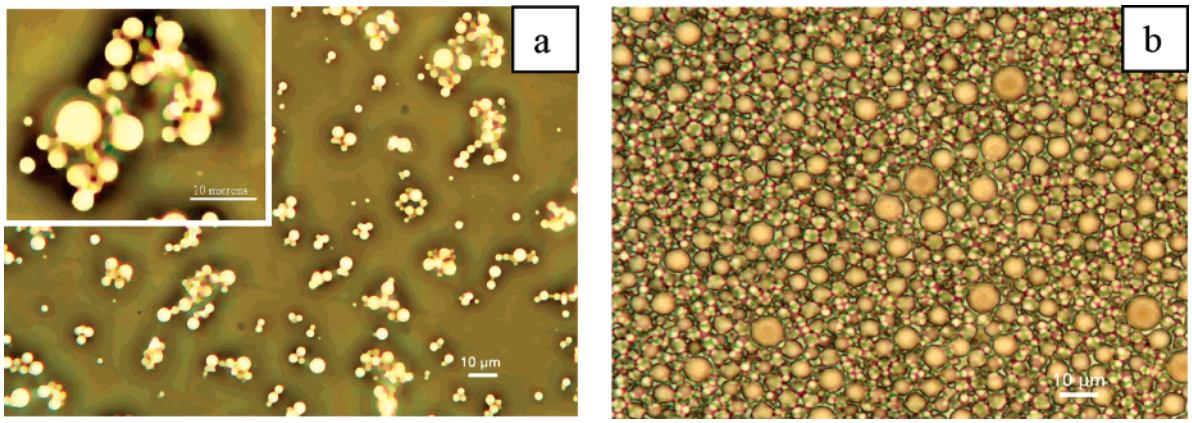

Figure 12. Optical microscopy pictures of emulsions prepared at intermediate (a) and high concentrations (b) of PFD.

References and Notes

(1) Shinoda, K. In *Principles of Solution and Solubility*; Lagowski, J. J., Ed.; M. Dekker, Inc.: New York and Basel, 1978; p 180.

(2) Kresge, C. T.; Leonowicz, M. E.; Roth, W. J.; Vartuli, J. C.; Beck, J. S. *Nature* **1999**, *359*, 710.

(3) Beck, J. S.; Vartuli, J. C.; Roth, W. J.; Leonowicz, M. E.; Kresge, C. T.; Schmitt, K. D.; Chu, C. T. W.; Olson, D. H.; Sheppard, E. W.; McCulle, S. B.; Higgins, J. B.; Schlender, J. L. *J. Am. Chem. Soc.* **1992**, *114*, 10834.

(4) Zhao, D.; Huo, Q.; Feng, J.; Chmelka, B. F.; Stucky, G. D. *J. Am. Chem. Soc.* **1998**, *120*, 6024.

(5) Zhao, D.; Feng, J.; Huo, Q.; Melosh, N.; Fredrikson, G.; Chmelka, B. F.; Stucky, G. D. *Science* **1998**, *279*, 548.

(6) Bagshaw, S. A.; Prouzet, E.; Pinnavaia, T. J. *Science* **1995**, *269*, 1242.

(7) Prouzet, E.; Pinnavaia, T. J. *Angew. Chem., Int. Ed. Engl.* **1997**, *36*, 516.

(8) Blin, J. L.; Léonard, A.; Su, B. L. *Chem. Mater.* **2001**, *13*, 3542.

(9) Corma, A. *Chem. Rev.* **1997**, *97*, 2373.

(10) Ciesla, U.; Schüth, F. *Microporous Mesoporous Mater.* **1999**, *27*, 131.

(11) Vallet-Regi, M.; Ramila, A.; Del Real, R. P.; Pérez-Pariente, J. *Chem. Mater.* **2001**, *13*, 308.

(12) Xu, X.; Tian, B.; Kong, J.; Zhang, S.; Liu, B.; Zhao, D. *Adv. Mater.* **2003**, *15*, 1932.

(13) Dai, Z.; Liu, S.; Ju, H.; Chen. H. *Biosens. Bioelectron.* **2004**, *19*, 861.

(14) Blin, J. L.; Gérardin, C.; Carteret, C.; Rodehüser, L.; Selve, C.; Stéb, M. J. *Chem. Mater.* **2005**, *17*, 1479.

(15) Firouzi, A.; Kumar, D.; Bull, L. M.; Besier, T.; Sieger, P.; Huo, Q.; Walker, S. A.; Zasadzinski, J. A.; Glinka, C.; Stucky, G. D. *Science* **1995**, *267*, 1138.

(16) Lee, Y. S.; Sujardi, D.; Rathman, J. F. *Langmuir* **1996**, *12*, 6202.

(17) Huo, Q.; Margolese, D. I.; Ciesla, U.; Feng, P.; Gier, T. E.; Sieger, P.; Leon, R.; Petroff, P. M.; Schüth, F.; Stucky, G. D. *Nature* **1994**, *368*, 317.

(18) Holland, B. T.; Blanford, C. F.; Do, T.; Stein, A. *Chem. Mater.* **1999**, *11*, 795.

(19) Sen, T.; Tiddy, G. J. T.; Casci, J. L.; Anderson, M. W. *Chem. Commun.* **2003**, 2182.

(20) Sen, T.; Tiddy, G. J. T.; Casci, J. L.; Anderson, M. W. *Microporous Mesoporous Mater.* **2005**, *78*, 255.

(21) Carn, F.; Colin, A.; Achard, M. F.; Deleuse, H.; Sellier, E.; Birot, M.; Backov, R. *J. Mater. Chem.* **2004**, *14*, 1370.

(22) Nakanishi, K.; Kobayashi, Y.; Amatani, T.; Hirato K.; Kodaira, T. *Chem. Mater.* **2004**, *16*, 3652.

(23) Amatani, T.; Nakanishi, K.; Hirato K.; Kodaira, T. *Chem. Mater.* **2005**, *17*, 2114.

(24) Blin, J. L.; Lesieur, P.; Stébé, M. J. *Langmuir* **2004**, *20*, 491.

(25) Han, Y.; Zhao, D.; Song, J.; Yang, X.; Li, N.; Di, Y.; Li, C.; Wu, S.; Xu, X.; Meng, X.; Lin, K.; Xiao, F. S. *Angew. Chem., Int. Ed.* **2003**, *42*, 3633.

(26) Tan, B.; Dozier, A.; Lehmler, H. J.; Knutson, B.; Rankin, S. E. *Langmuir* **2004**, *20*, 6981.

(27) Rankin, S. E.; Tan, B.; Lehmler, H. J.; Hindman, K. P.; Knutson, B. *Microporous Mesoporous Mater.* **2004**, *73*, 197.

(28) Groenewolt, M.; Antonietti, M.; Polarz, S. *Langmuir* **2004**, *20*, 7811.

(29) Shinoda, K.; Ogawa, T. *J. Colloid Interface Sci.* **1967**, *24*, 56.

(30) Barret, E. P.; Joyner, L. G.; Halenda, P. P. *J. Am. Chem. Soc.* **1951**, *73*, 37.

(31) Jarionec, C. P.; Kruk, M.; Jarionec, M. *Phys. Chem. B* **1998**, *102*, 5503.

(32) Decruppe, J. C.; Pontin, A. *Eur. Phys. J.* **2003**, *10*, 201.

(33) Langenfeld, A.; Celini, N.; Stébé, M. J. *Proceedings of the Third World Congress on Emulsions*; 2002; 1-F/192.

(34) *Emulsions and Solubilization*; Shinoda, K., Frieberg, S., Eds.; J. Wiley: New York, 1986.

(35) Gross, U.; Papke, G.; Rüdiger, S. J. *J. Fluorine Chem.* **1993**, *61*, 11.

(36) Kunieda, H.; Shinoda, K. *J. Colloid Interface Sci.* **1985**, *107*, 107.

(37) Ravey, J. C.; Stébé, M. J. *Prog. Colloid Polym. Sci.* **1988**, *76*, 234.

(38) Alibrahim, M.; Stébé, M. J.; Dupont, G.; Ravey, J. C. *J. Chim. Phys.* **1997**, *94*, 1614.

(39) Brunauer, S.; Deming, L. S.; Deming, W. S.; Teller, E. *J. Am. Chem. Soc.* **1940**, *62*, 1723.

(40) Dubinin, M. M. In *Progress in Surface and Membrane Science 9*; Cadenhead, D. A., Ed.; Academic Press: New York, 1975; p 1.

(41) Kipkemboi, P.; Fogden, A.; Alfredsson, V.; Flodström, K. *Langmuir* **2001**, *17*, 5398.

(42) Ravey, J. C.; Stébé, M. J.; Sauvage, S. *J. Chim. Phys.* **1994**, *91*, 259.